J Mater Sci: Mater Electron (2025) 36:184

Design and fabrication of nitrogen- and sulfur-doped carbon quantum dot-integrated cobalt hexacyanoferrate hybrid sensor electrodes for enhanced dopamine detection

D. Sivagurunathan[1], A. Padmapriya[1], M. Devendiran[2], and R. A. Kalaivani[1,*]

[1] *Department of Chemistry, School of Basic Sciences, Centre for Energy and Alternative Fuels, Vels University, Pallavaram, Chennai, Tamilnadu 600117, India*

[2] *Central Instrumentation Laboratory, Vels University, Pallavaram, Chennai, Tamilnadu 600117, India*

Received: 23 August 2024
Accepted: 7 January 2025

ABSTRACT

In this study, we present a novel composite electrode based on nitrogen and sulfur co-doped carbon quantum dots (NSCQDs), synthesized using *Senna auriculata* biomass, a natural and renewable source. X-ray diffraction (XRD) analysis revealed high crystallinity of the synthesized material, with the NSCQD signature being indistinct due to irregular stacking and low concentration. Scanning electron microscopy (SEM) confirmed the formation of larger spherical hybrid clusters, attributed to the incorporation of NSCQDs. We analyzed the composite electrode using cyclic voltammetry (CV) and differential pulse voltammetry (DPV), which revealed efficient electron transfer, minimal background current, and a broad detection range. The DPV analysis exhibited excellent linearity and sensitivity, with a proportional decrease in peak currents over a dopamine concentration range of 20–7000 nM. The sensor achieved a high sensitivity of 0.01521 μA/nM and a low detection limit of 0.1 nM. The modified electrode also demonstrated low noise and high reproducibility, underscoring its practical viability. This sustainable technique not only adheres to green chemistry principles, but it also improves the electrochemical characteristics of NSCQDs, making them extremely useful for dopamine sensing. The combination of NSCQDs and cobalt hexacyanoferrate (CoHCF) produced a composite electrode with high selectivity and sensitivity. The NSCQD/CoHCF composite electrode outperforms many existing sensor technologies and holds significant promise for reliable and efficient dopamine detection in real-world applications.

Address correspondence to E-mail: director.sbs@velsuniv.ac.in

https://doi.org/10.1007/s10854-025-14246-8
Published online: 22 January 2025

1 Introduction

In recent years, neurotransmitters are of great interest due to their vital roles within the central nervous system. Among these, dopamine ((3,4-dihydroxyphenyl) ethylamine, DA) is particularly significant as a key neurotransmitter and an important diagnostic marker. Dopamine is crucial for the proper functioning of the central nervous system as well as the renal and hormonal systems [1, 2]. This catecholamine neurotransmitter is especially noteworthy for its implications in treating disorders of the central nervous system, such as schizophrenia and Parkinson's disease. Imbalances in dopamine levels within the central nervous system can indicate the presence of neurological disorders [3]. High levels of dopamine are linked to cardiotoxicity, potentially causing rapid heart rates, hypertension, heart failure, and substance addiction. On the other hand, low dopamine levels are associated with stress and Parkinson's disease. Consequently, the precise and sensitive detection of dopamine is essential for the diagnosis of various mental health disorders [4, 5].

Electrochemical methods are a particularly good choice for DA concentration measurement because of their many advantages, including affordability, portability, ease of use, and quick detection times. Carbon electrodes and glassy carbon electrodes are commonly used in conventional electrochemical biosensors for the detection of DA [6]. However, these traditional electrodes have limitations in terms of electron transfer ability, sensitivity, and selectivity [7]. Recent advancements in electrochemical sensors aim to enhance these attributes by improving sensitivity, selectivity, and biocompatibility. Innovations in electrode materials and sensor design have led to more efficient and reliable electrochemical biosensors for dopamine detection. Transition metal hexacyanoferrates (TMHCFs) with the general composition $A^{a+}[Fe\ (CN)_6]^{b+}{\cdot}nH_2O$ are significant multicore inorganic polymers that have garnered attention in the electroanalytical chemistry field due to their remarkable magnetic, electrochromic, and electrochemical characteristics [8, 9]. These mixed-valence compounds exhibit numerous appealing properties, including electrocatalysis, electrochromic, ion-exchange selectivity, ion-sensing, and photomagnetic properties. Among the different TMHCFs, Cobalt Hexacyanoferrate (CoHCF) an analogue of Prussian Blue, stands out as one of the more interesting inorganic polymers [10]. In this compound, both iron and cobalt exhibit two oxidation states. The advantage of using CoHCF among the various TMHCFs lies in its excellent electrocatalytic properties and ion-exchange selectivity. Additionally, it shows well-defined electrochemical responses without undergoing dissolution due to redox phenomena or various diffusive processes, thereby maintaining charge neutrality. GCE with CoHCF modification have been used as biological sensors to measure glucose [11], ascorbic acid (AA) [12], and H_2O_2 [13]. Further, CoHCF has shown excellent electrocatalytic activity for dopamine oxidation, whose electrochemical behavior is well reported in previous studies [14, 15].

Recent research has demonstrated that carbon-based electrodes can achieve significant separation of the oxidation potentials for DA and AA. This capability enhances the selective detection of DA, even in the presence of up to 200 μM AA, and results in improved sensitivity as indicated by higher voltammetric current signals [16]. These benefits are attributed to the carbon-based electrodes' highly electroactive surface area and their rapid electron-transfer characteristics [17]. By allowing the adjustment of electrical characteristics and boosting structural stability, doping carbon materials with hetero atom is crucial for increasing their electrical conductivity, catalytic activity, and surface reactivity. This improves performance and adaptability in applications such as sensors, batteries, and catalysis [18]. Shiri and colleagues investigated a high-efficiency electrochemical sensing system utilizing a carbon paste electrode modified with a C-dots@$CuFe_2O_4$ nanocomposite for the precise measurement of rifampicin and isoniazid [19]. Hassine et al. conducted a study to improve the detection of DA using a glassy carbon electrode enhanced with graphene oxide, nickel, and gold nanoparticles. The modified electrode exhibited a linear detection range for DA from 2×10^{-7} M to 10^{-4} M, with a sensitivity of 0.641 A M^{-1} [20]. The detection limit was determined to be 10^{-7} M. Moreover, the modified electrode demonstrated high selectivity for DA even in the presence of common interfering substances such as uric acid (UA), AA, and glucose. carbon quantum dots (CQDs) are versatile nanomaterials prized for their biocompatibility, tunable fluorescence, and easy surface modification, finding applications in bioimaging, sensing, drug delivery, and catalysis [21, 22]. Their synthesis typically involves controlled carbonization or pyrolysis of carbon-rich sources like organic molecules, polymers, or biomass, often with surface doping or passivation to tailor their optical and chemical properties

[22–24]. *Senna Auriculata*, known as *Cassia Auriculata* is esteemed for its medicinal benefits in treating blood glucose levels, urinary disorders, ulcers, and skin conditions, owing to its high cellulose and lignin content. This makes it an ideal biomass source for CQDs synthesis. In our study, we use the sustainable and eco-friendly features of *Senna auriculata* biomass, a natural and renewable source high in cellulose (60%) and lignin (18%), to synthesize carbon quantum dots. *Senna auriculata*, well-known for its medicinal applications, is an excellent precursor for the production of N and S co-doped CQDs (NSCQDs) with superior electrochemical characteristics. By combining these NSCQDs with CoHCF, we synthesized a composite electrode for very sensitive and selective dopamine detection. Our study intends to investigate the efficacy of this green, biomass-derived composite electrode, emphasizing the benefits of employing doped carbon quantum dots obtained from natural sources.

2 Experimental methods

2.1 Materials

Polyvinyl Alcohol (PVA), potassium Hexacyanoferrate ($K_4[Fe(CN)_6$), and cobalt chloride ($CoCl_2$) were purchased from SRL Laboratories, Chennai, India. Pencil Graphite Electrodes were received from M/S Piramal Enterprises, Chennai. Additionally, essential acids, bases, and solvents used in this study were purchased from Merck India Ltd. All chemicals were used as received without further purification.

2.2 Synthesis of pristine and N, S co-doped carbon quantum dot

The *senna auriculata* flowers were collected from a nearby village in Chennai, close to Kalpakkam. Dust was removed from the flowers by air drying them, and then they were ground in a home mixer. The powdered *Senna Auriculata* was combined with distilled water in part. This combination was put through a hydrothermal reaction at about 180 °C for 6 h in a stainless-steel autoclave lined with Teflon. After the reaction, the oven was turned off and the autoclave was allowed to gradually cool to room temperature. The mixture was separated into four 15 mL centrifuge tubes when it had cooled, and it was centrifuged for 30 min at 2000 rpm. The remaining sediments were then clearly filtered out of the supernatant using micro filter paper. The synthesis of nitrogen and sulfur co-doped carbon quantum was accomplished via a similar method.

2.3 Synthesis of cobalt hexacyanoferrate and NSCQD/Cobalt hexacyanoferrate

Cobalt hexacyanoferrate was synthesized from cobalt chloride and potassium hexacyanoferrate by coprecipitation method. In this synthesis process, PVA acts as a stabilizing and binding agent, helping to stabilize and disperse the cobalt and hexacyanoferrate ions in solution. PVA guarantees a consistent particle distribution and improves the structural cohesiveness of the composite on the electrode surface by inhibiting early aggregation. Enhancing stability and attaining dependable, repeatable electrochemical performance depend heavily on this function. First, a 5 mL of cobalt chloride was dissolved in a 10% PVA solution with continuous stirring. Simultaneously, an aqueous solution of potassium hexacyanoferrate was prepared in a separate container. This prepared potassium hexacyanoferrate solution was gradually added to the cobalt chloride solution drop by drop with proper stirring occasionally. The formed brown precipitate was thoroughly washed with distilled water three times to remove excess potassium and chloride ions. The derived cobalt hexacyanoferrate was then dried at room temperature. To prepare the composite material, the composite was drop-cast onto a paraffin-impregnated graphite electrode (PIGE) for application studies. Within a glass tube was a mixture of carbon quantum dots (NSCQDs), ethanol, graphene, acetone, and a known amount of CoHCF. This mixture was thoroughly mixed and then treated with ultrasonic waves for approximately three hours. The NS CQD/CoHCF combination was ultrasonically agitated, and the resulting composite was separated by centrifugation. The composite was then filtered and thoroughly cleaned with distilled water to get rid of any remaining contaminants. To create a powdered form appropriate for additional characterization applications in the electrode field, the purified NS CQD/CoHCF were dried. The scheme of the synthesis is shown in Fig. 1.

2.4 Fabrication of NSCQD/CoHCF composite electrode

For fabrication, Pencil Graphite Electrodes were employed. Paraffin wax was infused into the porous material of these electrodes to improve stability and

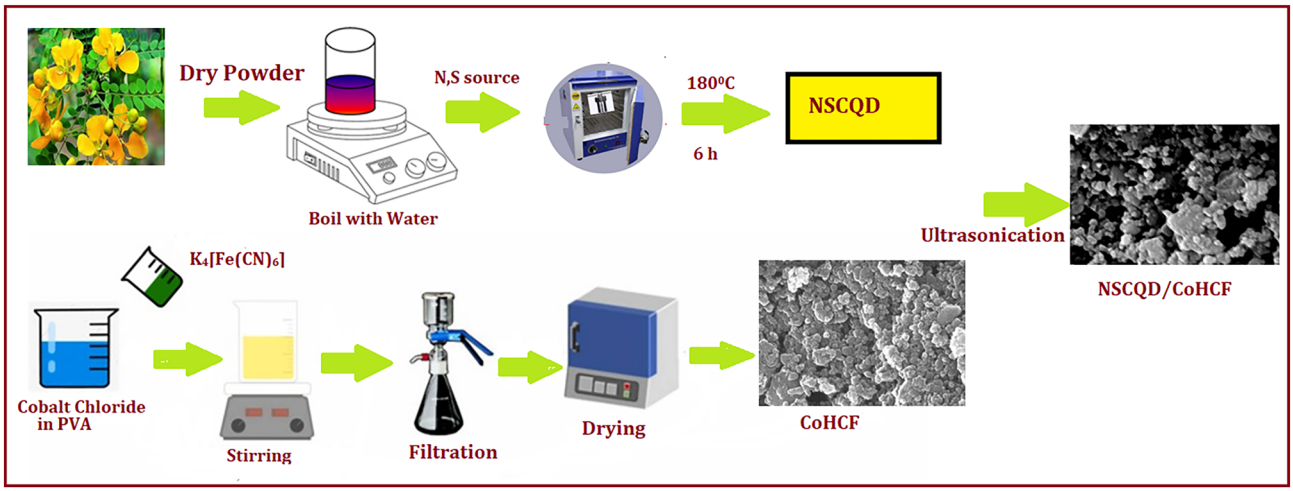

Fig. 1 Schematic illustration of synthesis of NSCQD/CoHCF hybrid composite

homogeneity during the coating procedures that followed. Each electrode was created with a separate circular area for drop-casting composites on one end, which was sharpened to act as the clamping or working electrode to facilitate different experimental approaches. The NSCQD/CoHCF composite was applied to this transparent circular area four to five times to ensure a uniform coating. To confirm the complete evaporation of any leftover solvent and complete adherence of the NSCQD/CoHCF composite, the electrodes were drop-cast and then allowed to cure overnight at room temperature. The electrodes were examined for integrity after drying.

2.5 Characterization

The crystal structure of the synthesized samples was determined using X-ray diffraction (XRD) analysis performed with a Rigaku Smartlab X-ray diffractometer equipped with a copper source (Cu Kα radiation, $\lambda = 1.54056$ Å) operating at 0.04 MV and 0.03 μA. The morphological characteristics were studied using a JEOL JEM-2100 Plus High-Resolution Transmission Electron Microscope (HRTEM), which includes imaging capabilities for both TEM and HRTEM. Additionally, Selected Area Electron Diffraction (SAED), Energy Dispersive X-ray Analysis (EDXA), and Scanning and Transmission Electron Microscopy (TEM) with mapping were employed during the analysis. Fourier Transform Infrared Spectroscopy (FTIR) using Spectrum Two FT-IR with Sp10 software from PERKIN ELMER, USA, was employed to verify the composition of CQDs and N, S CQDs. X-ray Photoelectron Spectroscopy (XPS) was utilized to obtain elemental chemical information and determine the concentration from the surface by using a Thermo Scientific ESCALAB 250xi.

3 Results and discussion

3.1 Crystalline phase analysis

X-ray diffraction analysis was used to ascertain the phase structure of the manufactured composite samples. The XRD patterns for NSCQD, virgin CQD, and the NSCQD/CoHCF composite are shown in Fig. 2. Regarding CQD, a wide peak detected at 23.2° is associated with the crystal plane index (002), signifying the aromatic and carbonized structures' parallel and azimuthal orientation [25]. Furthermore, a distinct peak is observed at 14.5°, which is ascribed to the (101) plane orientation, offering an additional perspective on the crystalline configuration of the CQDs. As opposed to CQD, NSCQD has a lower intensity of the 14.5° peak, which may indicate changes in crystal orientation or crystallinity. Additionally, a small peak at 27.5° that is not seen in CQD is shown in NSCQD, indicating the possibility of additional crystalline phases or structural changes brought about by the non-stoichiometric alteration. [26]. These findings illustrate the impact of non-stoichiometric modifications on the XRD properties of

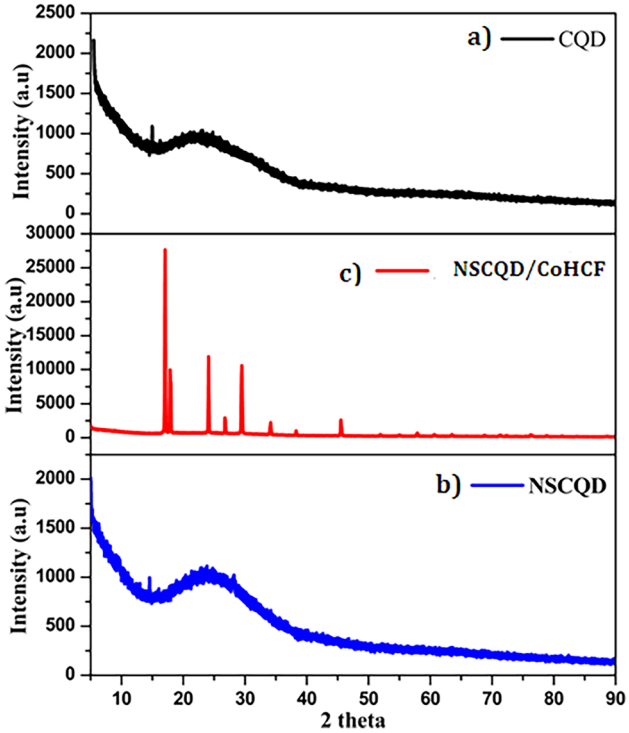

Fig. 2 Powder XRD patterns of **a** CQD **b** NSCQD **c** NSCQD/CoHCF

NSCQD. Although NSCQD shares some structural features with CQD, such as the broad (002) peak, there are notable differences in crystallinity and phase structure. Different diffraction peaks are visible at 2θ values of 21.5°, 29.12°, 41.2°, 40°, 46°, 49.1°, 57.6°, 59.1°, and 62.4° in the XRD investigation of NSCQD/CoHCF. The (200), (220), (400), (420), (422), (440), (600), and (620) crystal planes of the face-centered cubic (FCC) phase of CoHCF are represented by these peaks. As indicated by PDF 01–073-9927, the diffraction pattern is in perfect alignment with the cubic crystal structure of the FCC structure of CoHCF, which belongs to the space group Fm-3 m and has a lattice parameter of $a = 10.12$ Å. [27]. These observations are consistent with previously reported literature [28]. The XRD peaks are sharp and well-defined, indicating a high degree of crystallinity in the synthesized material. The characteristic peak of NSCQD is not visible in the NSCQD/CoHCF composite pattern, likely due to the low concentration and irregular stacking of the carbon dots. Additionally, the absence of extra diffraction peaks suggests that the products are of high purity. The crystallite sizes of the synthesized materials were determined using the Scherrer formula [29]:

$$D = \frac{k\lambda}{\beta \mathrm{Cos}\theta}$$

In this equation, D indicates crystallite size, K is the form factor (0.9), λ is the X-ray source wavelength, β is the full width at half maximum (FWHM) of the most intense diffraction peak, and θ is the Bragg angle. Using this method, the calculated crystallite sizes for the CQD, NSCQD, and NSCQD/CoHCF samples were 7 nm, 8 nm, and 12 nm, respectively. These findings suggest that introducing NSCQD into the CoHCF matrix causes an increase in crystallite size. In comparison to the NSCQD/CoHCF composite, the CQD and NSCQD samples have lower crystallite diameters, indicating a more finely divided or less crystalline structure. The bigger crystallite size in the NSCQD/CoHCF composite could be attributed to CoHCF's more stable crystal structure, which provides a solid framework for integrating NSCQD and resulting in a higher total crystallite size. When comparing the NSCQD/CoHCF composite to the individual CQD and NSCQD samples, the increased crystallite size indicates a better degree of crystallinity and perhaps superior structural integrity.

3.2 Vibrational and functional characteristic analysis

The characterization of NSCQD/CoHCF composites was further confirmed through the use of FTIR spectroscopy. The resulting spectra for CQD, NSCQD, and NSCQD/CoHCF are shown in Fig. 3a–c, respectively. The CQD spectrum in Fig. 3a exhibits a peak at around 3340 cm^{-1}, which is indicative of the –OH stretching vibration mode. Additionally, the C=O stretching vibration is correlated with a vibrational absorption band around 1640 cm^{-1} [30]. The absence of symmetric and asymmetric peaks of CH_2 at 2921 cm^{-1} and 2851 cm^{-1}, respectively, indicates that the carbon source was fully carbonized, transforming the hydrocarbon into a graphitic structure [31]. Moreover, a small peak at 2240 cm^{-1}, likely representing the –C≡N stretching vibration, suggests the presence of amino-containing functional groups [32]. The similar peaks between NSCQD and CQD, as shown in Fig. 3b, indicate that the primary carbon structure is largely retained in the doped material. The weak

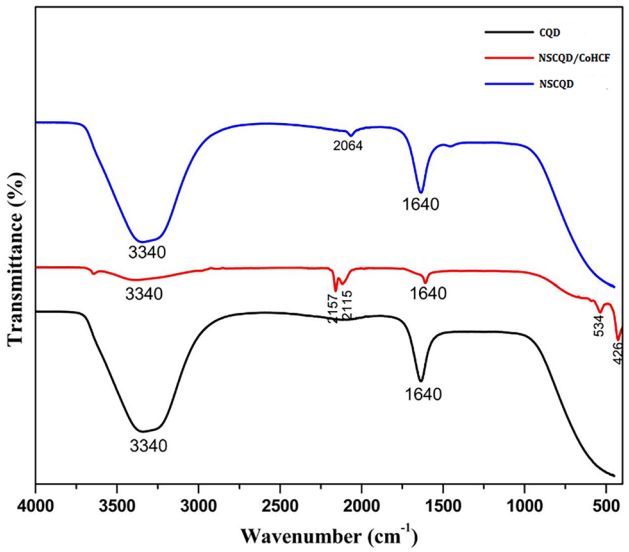

Fig. 3 FTIR spectra of of **a** CQD **b** NSCQD **c** NSCQD/CoHCF

peak at 2064 cm^{-1} suggests the introduction of nitrogen and sulfur atoms, leading to new chemical bonds or slight structural modifications. In the spectrum of NSCQD/CoHCF, the band at 2157 cm^{-1} corresponds to the typical characteristic absorption band of metal hexacyanoferrate, indicating the stretching vibration of the C≡N group in pure CoHCF [33, 34]. The symmetrical and asymmetrical –OH stretching vibration is also responsible for a large band in the 3300–3400 cm^{-1} area, which suggests the existence of water molecules in the composite. The stretching vibration of the Fe–CN–Co bonds is responsible for a prominent absorption band at 2115 cm^{-1} that is indicative of the Prussian Blue structure and indicates the successful development of the Fe–CN–Co linkage inside the composite. Moreover, the integration of CoHCF inside the NSCQD matrix is confirmed by the existence of distinctive peaks at 426 and 534 cm^{-1}. All of these results point to the NSCQD/Co-HCF composite's effective synthesis and integration with the intended structural elements.

3.3 Morphological analysis

SEM and TEM techniques were used to examine the morphological and structural properties of CoHCF and NSCQD/CoHCF composites, as illustrated in Figs. 4 and 5, respectively. A well-conducted synthesis process is indicated by the homogenous, monodisperse, and evenly distributed spherical particles with an average diameter of about 50 nm that are visible in the SEM image of CoHCF Fig. 4a. In contrast, the SEM image of the NSCQD/CoHCF composite Fig. 4b reveals larger spherical particles, with a noticeable increase in size compared to pristine CoHCF. This increase in particle size can be attributed to the successful integration of NSCQDs, which promotes the formation of larger hybrid clusters. The uniform dispersion and spherical morphology of NSCQD/CoHCF emphasize that the incorporation of NSCQDs was carefully controlled, leading to a homogeneous and stable composite. This comparison illustrates the tunability of the composite's morphology, which can be tailored by adjusting the NSCQD loading for specific applications. The hybrid material's elemental composition is further validated by the NSCQD/CoHCF composite's EDX analysis Fig. 4c. The presence of Co, Fe, C, N, and S in the EDX spectrum confirms that NSCQDs were successfully integrated into the CoHCF matrix. A consistent dispersion of NSCQDs within the CoHCF framework is indicated by the homogeneous distribution of these elements throughout the composite. Further morphological characteristics were obtained from TEM and HRTEM images (Fig. 5). The TEM image of NSCQD (Fig. 5a) shows well-defined, small, and uniform nanoparticles, demonstrating a high degree of size control and uniformity. The surface texture appears rougher, likely due to N and S doping, which modifies the surface characteristics of the NSCQDs. The TEM image of CoHCF (Fig. 5b) reveals spherical particles with a relatively smooth and homogeneous surface. When NSCQDs are integrated into the CoHCF matrix, as depicted in Fig. 5c, the resulting composite structure features larger, more intricate spherical clusters. The crystallinity and structural integration of NSCQDs inside the CoHCF matrix are examined in greater detail in the HRTEM picture of the NSCQD/CoHCF composite (Fig. 5d). The image shows distinct lattice fringes, which are a sign of the composite's high crystallinity. The CoHCF structure's (400) plane is represented by the measured lattice spacing, which is roughly 0.231 nm. The improved structural integrity and stability of the composite are a result of this spacing, which validates the NSCQDs' strong alignment and integration inside the CoHCF framework.

3.4 Chemical composition and surface state analysis

The X-ray photoelectron spectroscopy (XPS) analysis of NSCQD/CoHCF provides detailed insights into its

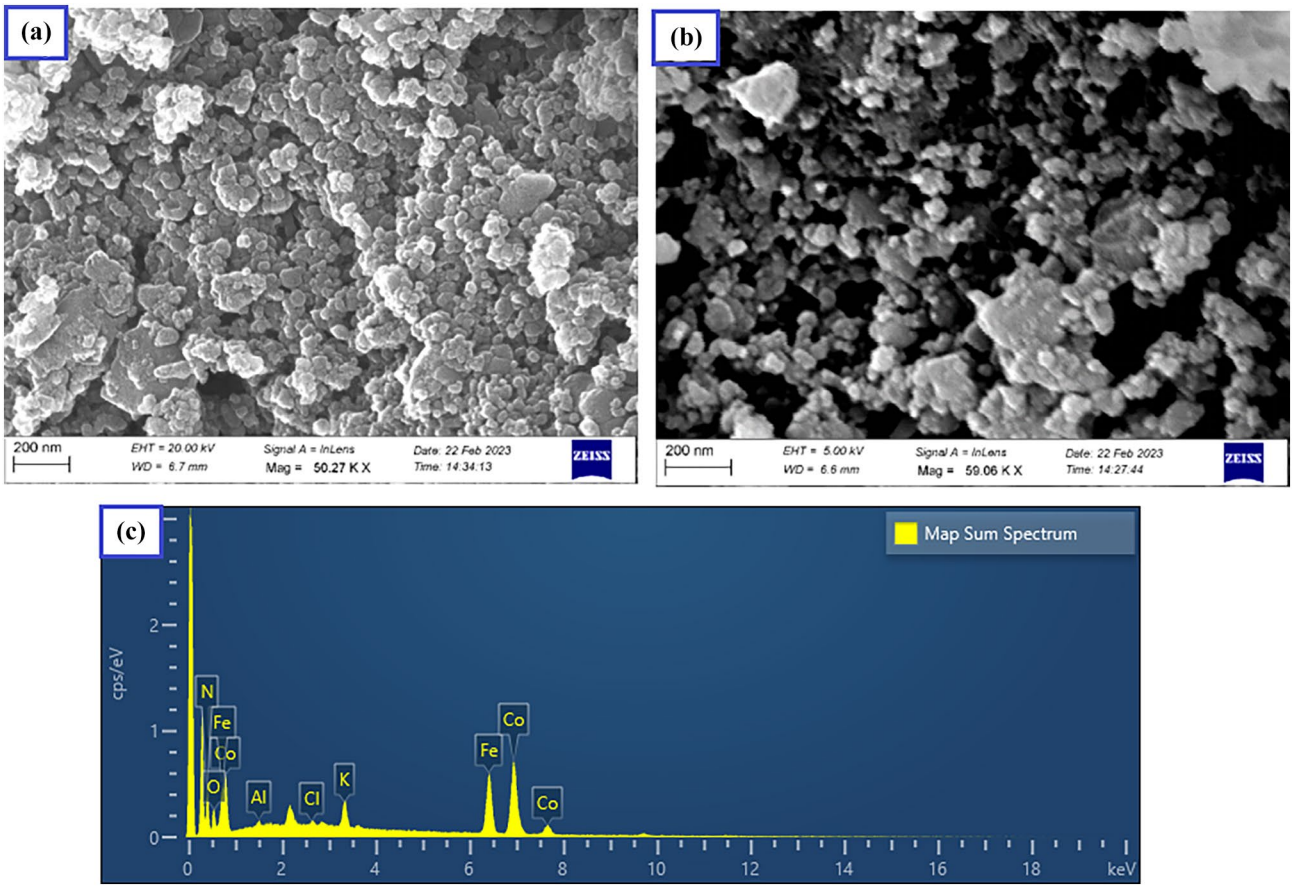

Fig. 4 SEM images of **a** CoHCF **b** NSCQD/CoHCF **c** EDAX spectrum of NSCQD/CoHCF

surface chemical composition and electronic structure. The survey scan spectrum (Fig. 6a) confirms the presence of Co, Fe, C, N, and S elements, indicating the comprehensive elemental composition of the sample. The high-resolution Co 2p spectrum (Fig. 6b) reveals peaks at 780.74 eV (Co $2p_{3/2}$) and 789.34 eV (Co $2p_{1/2}$), characteristic of Co^{2+} ions, suggesting the oxidation state and coordination environment of cobalt within the composite [35]. Similarly, the Fe 2p spectrum (Fig. 6c) shows peaks at 709.4 eV and 720.9 eV, corresponding to Fe^{2+} ions, indicating the presence of iron in a specific chemical environment within the composite material [36]. In the C 1 s spectrum, peaks at 284.3 eV (adventitious carbon, C–H, or C≡N), 285.1 eV (C–O), and 286.4 eV (C═O) reveal various carbon bonding states, providing insights into the surface functionalities and chemical groups present [37]. The N1s XPS spectrum of nitrogen-doped cobalt hexacyanoferrate reveals a main peak at 399.6 eV attributed to cyanide nitrogen (C≡N), along with additional peaks at 401.2 eV indicating doped nitrogen species like pyridinic nitrogen or nitrogen bonded to cobalt, and at 401.8 eV signifying graphitic or oxidized nitrogen introduced by doping (Fig. 6e). Moreover, the S 2p peaks at 158.9, 161.6, and 163.8 eV in the NSCQD/CoHCF composite show sulfur in several states: 158.9 eV indicates less sulfur interaction with metal centers, 161.6 eV indicates metal-sulfur bonding with cobalt or iron, and 163.8 eV depicts sulfur in organic or mildly oxidized forms, which improves electron transport and stability (Fig. 6f) [38, 39]. From the results, the elemental composition, oxidation states of metal ions (Co^{2+} and Fe^{2+}), surface functional groups of carbon, and chemical states of nitrogen and sulfur in the NSCQD/CoHCF composite, providing comprehensive understanding of its surface chemistry and electronic structure.

3.5 Dopamine detection performance analysis by cyclic voltammetric analysis

The electrochemical sensing capabilities of the NSCQD and CoHCF composite for dopamine

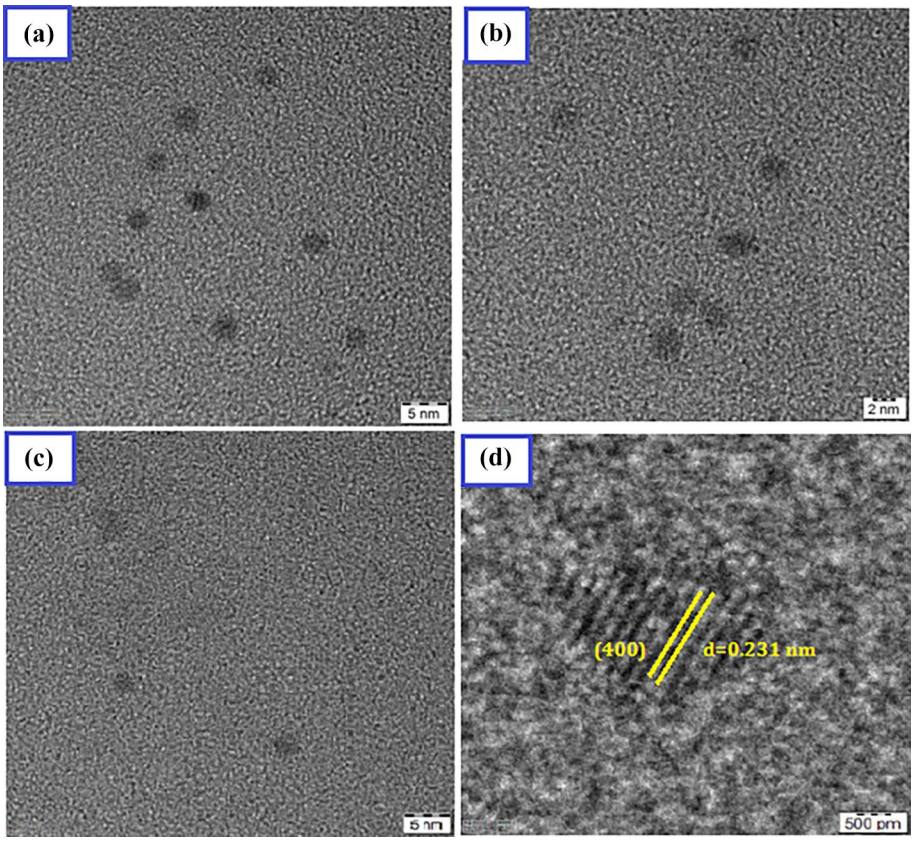

Fig. 5 TEM images of **a** CQD **b** NSCQD **c** NSCQD/CoHCF **d** HRTEM image of NSCQD/CoHCF

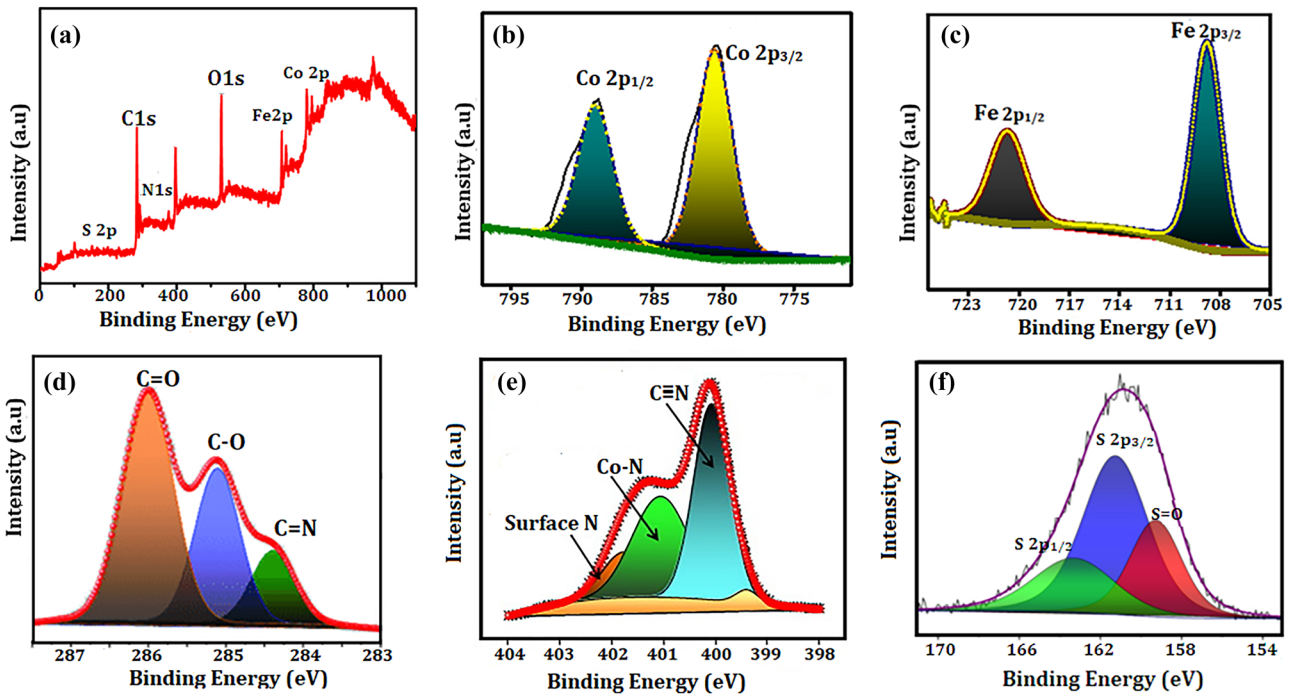

Fig. 6 XPS spectra **a** Survey scan spectra of NSCQD/CoHCF; High-resolution spectra of **b** Co 2p **c** Fe 2p **d** C 1 s **e** N 1 s **f** S 2p

detection were investigated using cyclic voltammetry (CV) with freshly prepared electrolytes and modified pencil graphite electrodes (PGEs) as working electrodes. The outcomes showed important characteristics such a broad potential window, low background currents, repeatability, and quick electron transfer kinetics. We monitored the dopamine oxidation peak current in order to examine the impact of scanning rate (from 10 to 100 mV s^{-1}). The peak current showed a linear increase with scan rates ranging from 10 to 100 mV/s. The best responses were obtained at a scan rate of 50 mV s^{-1}, which was chosen for further studies. Figure 7 presents CV results for dopamine solutions at concentrations ranging from 10 µL to 100 mL in a 0.01 M phosphate buffer (pH 7), with a scan rate of 50 mV s^{-1}. The CV examination of the NSCQD/CoHCF-modified PG electrode revealed distinct redox peaks, indicating effective electron transfer and molecular mobility. The CV of the fabricated hybrids on the PGE exhibited two distinct sets of redox peaks, which can be attributed to the redox processes of cation-free CoHCF and cation-rich CoHCF, indicating that the electrode's electrochemical behavior is modulated by the differing cation content within the CoHCF structures; additionally, the CV responses confirm that there is no electrochemical activity observed in the fabricated electrodes when dopamine is not added to the PBS buffer, highlighting the specificity of the electrodes toward dopamine detection. Moreover, a strong cathodic peak observed at − 0.4 V, indicating that dopamine was reduced to dopamine-o-quinone, while higher currents around + 1.0 V were associated with dopamine oxidation to dopamine-o-quinone [40, 41]. At higher dopamine concentrations, a unique irreversible oxidation peak was observed at 1.3 V, most likely due to the oxidation of the hydroxyl group on the aromatic ring of dopamine. The electrode produced a peak current of 1.3 mA at a lower potential of 0.65 V, demonstrating its robust electrocatalytic properties and increased conductivity. This performance indicates that the NSCQD/CoHCF-modified PG electrode has higher catalytic activity than standard electrodes, which frequently exhibit lower peak currents and less pronounced redox characteristics under identical conditions [42]. The findings illustrate the modified electrode's potential for successful dopamine detection, emphasizing the benefits of utilizing NSCQD and CoHCF in the modification procedure. In addition, specific oxidation and reduction peaks were also visible in the CV results. Additionally, a steady increase in current was observed with the increasing concentration of DA. The inset of Fig. 7 shows the linear calibration plot of DA concentration versus the redox peak current, described by the equations $I_{pa} = 1.0091x - 14.423$ ($R^2 = 0.9995$) and $I_{pc} = 0.839x + 9.897$($R^2 = 0.9976$), demonstrates the exceptional electrocatalytic behavior of the NSCQD/CoHCF-modified electrode for DA detection, as indicated by the strong linearity and sensitivity [43]. The linear relationship between anodic peak current and cathodic peak current and

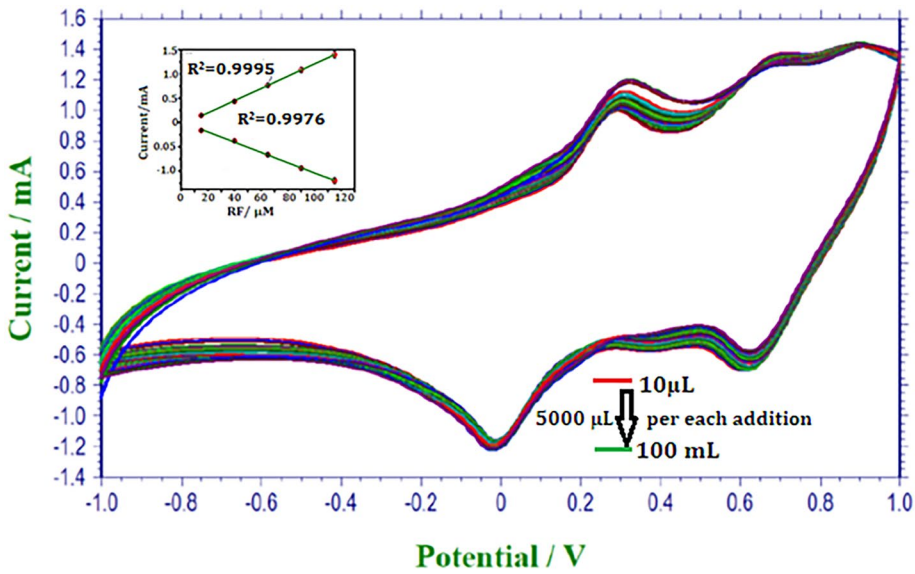

Fig. 7 Cyclic voltammograms of 10 µL to 100 mL of dopamine and 0.01 M PBS (pH 7.0) at NSCQD/CoHCF-modified PGE at a scan rate of 50 mV/s; Fig 7 (inset) Linear relationship of Ipa and Ipc vs dopamine concentration

increasing peak-to-peak separation at higher scan rates suggests that the electrochemical process is surface-controlled. The Randles–Sevcík equation was used to calculate the surface area of the NSCQD/CoHCF-modified PG electrode, and the result was 0.42 cm^2 [44]. With more active sites available for electrochemical reactions, this increase in surface area suggests that the change greatly expands the PG electrode's effective area. Because of this enhancement, electron transport is more effectively accomplished, improving sensor sensitivity. The sensor's capacity to precisely monitor dopamine levels within the specified range is confirmed by the linear relationship between peak currents and dopamine concentration, which is essential for real-world applications. The electrode's sensitivity and effective electron transfer kinetics are highlighted by the periodic shifts in peak currents, and its dependability is demonstrated by the low background current. Additionally, the steady potential window at various dopamine concentrations confirms the wide potential range of the sensor, which is essential for consistent measurements [45]. The NSCQD and CoHCF composite-modified electrodes are effective at detecting dopamine, as demonstrated by these CV data, which qualify them for use in biochemical analysis and clinical diagnostics.

3.6 Dopamine detection performance analysis by DPV analysis

The differential pulse voltammetry (DPV) method has various advantages, including operational simplicity, excellent sensitivity and accuracy, and a broad linear range for dopamine detection. As a result, DPV was used to evaluate the dopamine sensing capabilities of the NSCQD/CoHCF-modified PG electrode in ideal conditions. Figure 8 depicts the DPV responses of the NSCQD/CoHCF-modified PG electrode at dopamine concentrations ranging from 20 to 70,000 nM. The addition of 0.02 µM dopamine (DA) resulted in a unique oxidation response, with peak currents gradually increasing with greater DA concentrations. The peak current for DA oxidation increased linearly between 0.02 and 52 µM, with a correlation value (R^2) of 0.9889, showing acceptable linearity. This linearity is critical for accurate dopamine detection in real samples because it allows for proportional variations in oxidation peak currents with increasing dopamine content. The sensor's sensitivity was determined from the slope of the calibration curve (current response vs. DA concentration) using the following equation [46]:

$$Sensitivity = \frac{\Delta I}{\Delta C}$$

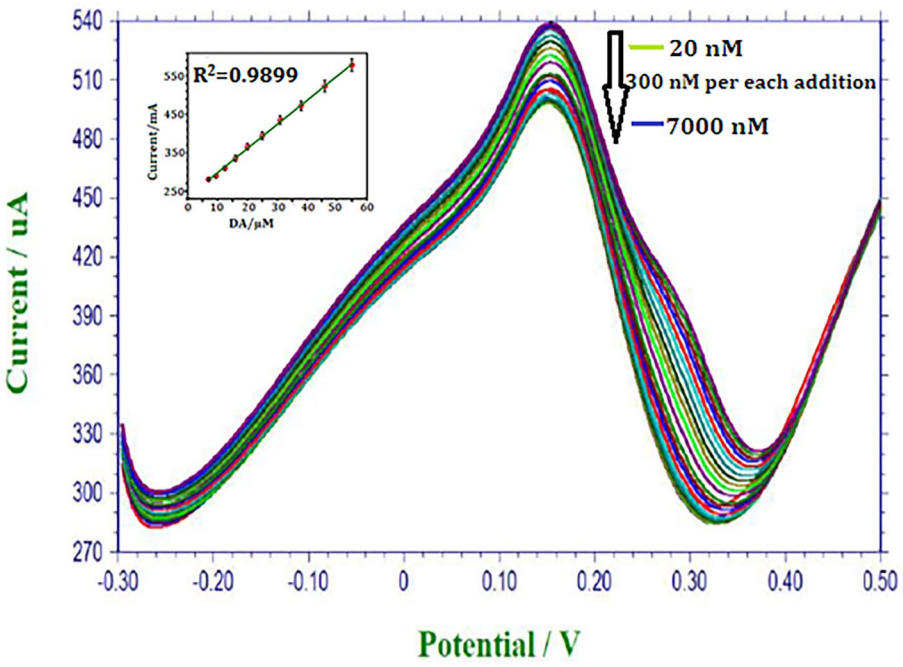

Fig. 8 DPV responses at the NSCQD/CoHCF-modified PG electrode for dopamine concentrations ranging from 20 to 7000 nM. Fig 8 (inset) Linear relationship of peak current vs dopamine concentration

where ΔI is the change in peak current (μA), ΔC is the change in dopamine concentration (nM). The inset of Fig. 8 further illustrates that the electrical signal change is linear with the logarithm (log) of the DA concentration, spanning a linear range from 20 to 70,000 nM. The regression equation obtained for this relationship is, $y(\mu A) = 1.7689 \times \log(C\ DA) + 11.522$ with $R^2 = 0.9899$, with a correlation coefficient $R^2 = 0.9899$. This regression equation validates the strong linear relationship between DA concentration and the current response, facilitating accurate trace-level dopamine quantification. The detection limit (LOD) was calculated according to IUPAC standards, defined as: $LOD = \frac{3\sigma}{s}$ where, σ is the standard deviation of the blank measurements (noise level), S is the slope of the calibration curve (sensitivity) [47]. Using this formula, the sensor demonstrated a sensitivity of 0.01521 μA/nM and a detection limit of 0.1 nM, underscoring its capability to detect even minute quantities of dopamine. The consistent rise in peak currents during DPV measurements also indicates the NSCQD/CoHCF-modified PG electrode's excellent repeatability, providing reliable readings with minimal noise. This low-noise characteristic enhances measurement accuracy, particularly for trace dopamine detection. Additionally, the stable potential window observed across varying concentrations demonstrates the electrode's robustness and reliability in electrochemical sensing [48]. The DPV analysis of the NSCQD/CoHCF composite electrode demonstrated highly favorable electrochemical responses, which are crucial for dopamine sensing applications. The DPV results showed a clear, proportional decrease in peak currents across a dopamine concentration range of 20 to 7000 nM, indicating excellent linearity and consistent performance. The composite electrode exhibited a high sensitivity of 0.01521 µA/nM, with a low detection limit of 0.1 nM, underscoring its potential for ultra-trace detection of dopamine. Additionally, the minimal background current and high peak current stability observed in DPV further confirm the efficient electron transfer within the NSCQD/CoHCF composite. These responses suggest that the composite electrode design provides a significant advantage in terms of sensitivity and specificity, making it a competitive choice for real-world dopamine detection applications. A comparative analysis of the NSCQD/CoHCF composite electrode with other reported electrode materials for dopamine detection is presented in Table 1 [12, 49–56]. This table summarizes the detection limits, linear ranges, and detection methods of various electrode materials, including porphyrin-functionalized graphene, boron-doped diamond, and several transition metal hexacyanoferrate (TMHCF) hybrids. As shown in Table 1, our NSCQD/CoHCF composite demonstrates a notably low detection limit of 0.1 nM and an extended linear range of 20 to 7000 nM, which are superior to most reported values. In comparison, other materials, such as graphene-modified GCE and boron-doped diamond electrodes, exhibit higher detection limits of 2.64 µM and 0.05 µM, respectively, while other TMHCF-based electrodes, such as the nickel hexacyanoferrate/poly(1-naphthol) hybrid, reach a detection limit of 2.1×10^{-8} M, which is still higher than our composite. Furthermore, the

Table 1 Comparison results of present work with previously published work toward dopamine detection applications

Electrode materials	Detection method	Detection limit	Linear range	Reference
Porphyrin-functionalized graphene	DPV	0.01 µM	0.01–200 µM	[49]
Polyethyleneimine	Fluorescence	0.3 µM	1–200 µM	[50]
Graphene-modified GCE	Electrochemical	2.64 µM	4 µM–100	[51]
Boron-doped diamond	Electrochemical	0.05 µM	5–250 µM	[52]
Nickel hexacyanoferrate /poly(1-naphthol) hybrid	Electrochemical three electrode system	2.1×10^{-8} M	0.1–4.3 µM	[53]
Nanostructure Ruthenium Oxide Hexacyanoferrate/ Ruthenium Hexacyanoferrate hybrid	Electrochemical	0.195×10^{-7}µMDA	0.5–550 µM	[54]
Cobalt–Nickel hexacyanoferrate	Electrochemical	1.5×10^{-8} M	0.2–500 µM	[12]
Cerium Hexacyanoferrate (III) Nanoparticle-modified Carbon Paste Electrode	DPV	$1.9 \times 10 - 7$	9.0×10^{-7} to 8.0×10^{-6} mol/L	[55]
Nickel Hexacyanoferrate and Bentonite Clay	Electrochemical	1.5 µM	25–1000 µM	[56]
NSCQD/CoHCF	Electrochemical	0.1 nM	20 to 7000 nM	This work

NSCQD/CoHCF composite's broader linear range surpasses that of many alternatives, such as cerium hexacyanoferrate-modified carbon paste electrodes, which have a range of 9.0×10^{-7} to 8.0×10^{-6} mol/L. This comparison emphasizes that the NSCQD/CoHCF composite electrode is highly effective for ultra-trace detection of dopamine, combining low detection limits with an extensive linear range, and demonstrating the robustness and practical viability of our approach for real-world dopamine sensing applications.

3.7 Selectivity and sensitivity analysis

Dopamine and uric acid were used as interferant molecules to test the developed biosensor's selectivity. The rationale behind selecting these compounds is that they coexist in fluid environments, such as blood and cerebrospinal fluid, making their simultaneous detection essential for comprehensive monitoring and diagnosis. Clinical uses hinge on the sensor's capacity to accurately identify and quantify these chemicals. Stepwise increasing quantities of uric acid were combined with 1 mL of dopamine in an experiment to assess the sensor's selectivity and sensitivity. This method ensured the sensor's usability in actual clinical diagnostics by allowing for the evaluation of its ability to detect and distinguish between the two analytes. In this DPV investigation, the NSCQD/CoHCF-modified PG electrode was evaluated for the simultaneous detection of DA and UA. The investigation involved changing the concentrations of these two analytes. In Fig. 9a, the DPV profiles were generated by changing the concentration of DA from 0.1 to 70 μM while maintaining the UA concentration constant at 0.1 μM. A linear correlation coefficient (R^2) of 0.9946 was found between the oxidation peak current (Ipa) and DA concentrations. The detection limit for DA was 0.016 μM, and the sensor's sensitivity was calculated to be 3.347 μA μM^{-1} cm^{-2}. Figure 9b shows a linear connection between UA concentrations ranging from 0.1 to 70 μM and DA concentrations at 1.0 μM. The presence of DA had no effect on the DPV profiles obtained under these conditions. A linear regression equation with a correlation coefficient (R^2) of 0.9957 was established (inset of Fig. 9b). The NSCQD/CoHCF-modified PGE sensor has a sensitivity of 0.632 μA μM^{-1} cm^{-2} and a detection limit of 0.016 μM for UA. The NSCQD/CoHCF-modified PG electrode demonstrated high sensitivity and linearity for the simultaneous detection of dopamine and uric acid, achieving detection limits of 0.012 μM for DA and 0.016 μM for UA. The obtained results further confirmed by CV results In the CV experiment, the NSCQD/CoHCF-modified PG electrode was investigated for its ability to detect UA and DA. The study was divided into two parts: first, incrementally raising the concentration of uric acid while maintaining a constant dopamine concentration, and second, progressively increasing dopamine levels with a fixed uric acid concentration. The results, shown in Fig. 10a, b, indicate distinct and separate oxidation peaks for uric acid and dopamine, demonstrating the electrode's ability to distinguish between

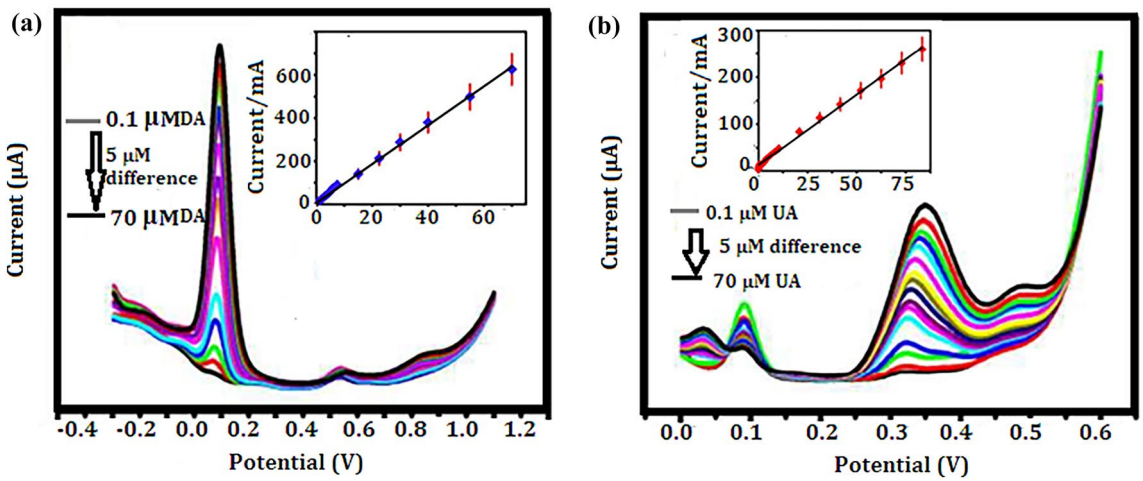

Fig. 9 DPV results of NSCQD/CoHCF/PGE **a** for varied concentration of DA with fixed concentration of UA. **b** for varied concentration of UA with fixed concentration of DA

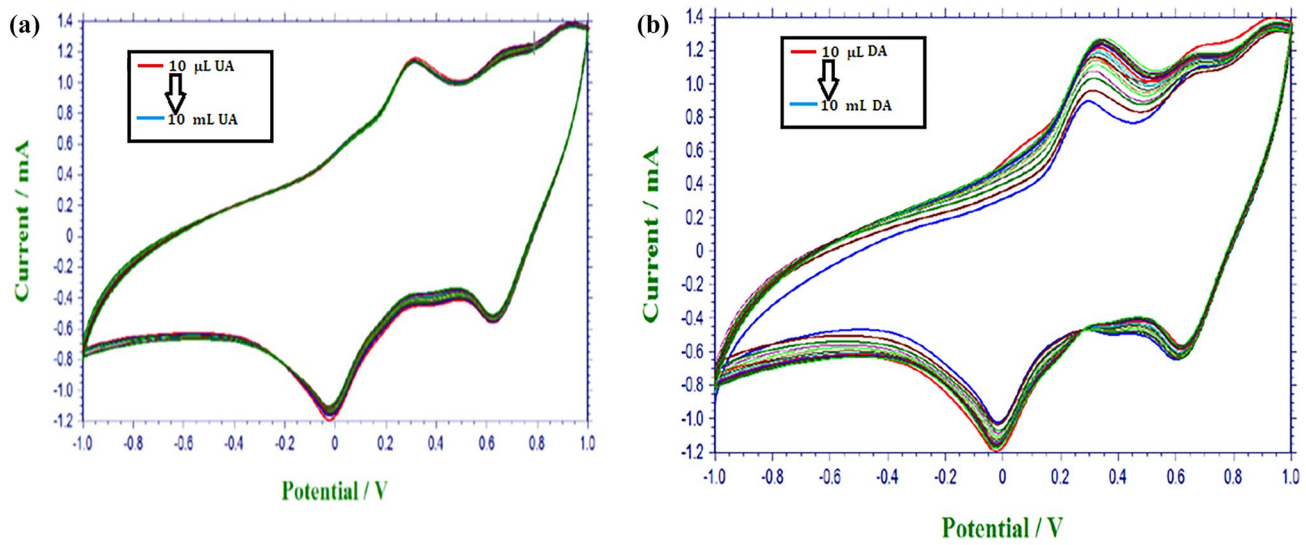

Fig. 10 Cyclic voltammograms of; **a** stepwise increase of uric acid with 1 ml of dopamine **b** stepwise increase of dopamine with 1 ml of uric acid

these analytes [57, 58]. The sensor's great sensitivity was demonstrated by peak shifts and increases in peak currents as analyte concentrations increased. The electrode's selectivity and reliability make it a promising tool for detecting these analytes in complex samples.

3.8 Stability and recyclability analysis

For the NSCQD/CoHCF composite to be used practically in dopamine sensing, stability and recyclability are essential. By analyzing the electrochemical performance of the NSCQD/CoHCF-modified electrode throughout several cycles of use, the stability of the CQDs within the composite was evaluated. After several cycles, the composite's performance barely degraded, suggesting that the NSCQDs are firmly incorporated into the CoHCF matrix. The strong connection between NSCQDs and CoHCF, which inhibits leaching and preserves the structural integrity of the composite under electrochemical conditions, is responsible for this stability. By using the same electrode for several dopamine detection cycles, recyclable materials were further assessed. As shown in Fig. 11a, with a retention of almost 95% of its initial sensitivity after 10 successive cycles, the NSCQD/CoHCF combination showed good recyclability. Because of its recyclability, the composite is suited for real-world applications where long-term operational stability is crucial because it demonstrates its resilience and capacity for recurrent usage. Thus, the CQDs' stability and recyclable nature in the composite support the material's applicability as a trustworthy electrochemical sensor. Moreover, the lifetime of NSCQD/CoHCF-modified electrodes was assessed by tracking its electrochemical performance over long stretches of time and numerous cycles. After extended use in dopamine detection over a period of 30 days, the electrode maintained roughly 92% of its initial sensitivity. This consistent performance implies that the NSCQDs are firmly incorporated into the CoHCF matrix, halting the active material's quick deterioration or leaching. Additionally, the electrode's endurance is attributed to the strong contact between NSCQDs and CoHCF, which sustains its electrochemical response over time with no signal drift. This durability demonstrates the NSCQD/CoHCF composite electrode's suitability for long-term dopamine sensing applications.

3.9 Practical and real-world setting analysis

To validate the sensor's performance in practical, real-world settings, we analyzed a dopamine sample collected from a clinical laboratory, with the CV results presented in Fig. 11b. The CV results for the incremental addition of the clinical dopamine sample exhibit trends similar to those observed with the chemically prepared sample. The distinct oxidation and reduction peaks, along with the increasing anodic and cathodic peak currents as dopamine concentration rises, confirm that the prepared electrode effectively responds

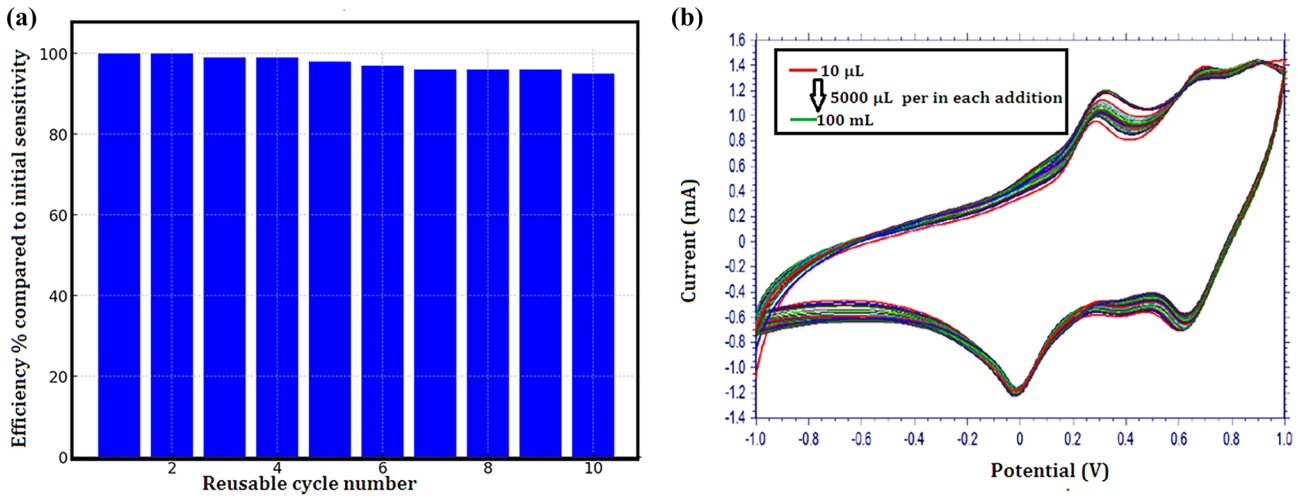

Fig. 11 **a** Reusability test of NSCQD/CoHCF/PGE **b** Cyclic voltammograms of 10 µL to 100 mL of clinical dopamine and 0.01 M PBS (pH 7.0) at NSCQD/CoHCF-modified PGE at a scan rate of 50 mV/s

to varying dopamine levels in clinical samples. The consistent peak current shifts and stable potential window across different dopamine concentrations in the clinical sample demonstrate the electrode's sensitivity, efficient electron transfer kinetics, and broad potential window. These features demonstrate the sensor's dependability and applicability for precise measurements in actual biological samples. The electrode's durability and potential for useful applications in clinical diagnostics are highlighted by this stability test. Furthermore, genuine dopamine and artificial dopamine have comparable CV forms. The quantity of active sites is measured using the electrochemical double-layer capacitance (Cdl) [59, 60]. According to the computed data, NSCQD displays a Cdl value of 17.5 mF cm^{-2} for genuine dopamine, which is greater than 16.2 mF cm^{-2} for chemical dopamine. Real dopamine greatly expands the area of CV at the same sweeping speed as pharmaceutical dopamine. This suggests that actual dopamine increases the electrode's active surface area and electrochemical reactivity, supporting the effectiveness of as synthesized NSCQD/CoHCF as sensor electrode for ultrasensitive detection of dopamine.

3.10 Mechanism of enhancement in dopamine detection

The enhanced electrochemical performance of the NSCQD/CoHCF composite arises from a combination of interfacial and defect effects that synergistically improve electron transfer, increase active sites, and boost material reactivity. As N and S co-doped carbon quantum dots (NSCQDs) are incorporated into the CoHCF matrix, strong interfacial contacts are produced, resulting in effective electron transport channels that lower resistance and limit electron–hole recombination [61]. For the purpose of improving conductivity and general electrochemical behavior, this tight connection guarantees quick and steady electron movement. In addition to adding more active sites for electrochemical reactions, the introduction of N and S dopants into the carbon quantum dots introduces a variety of structural defects and heteroatom functional groups. These defects act as additional active sites for electrochemical reactions, significantly increasing the reactivity of the composite material. N and S doping modifies the electronic structure of the carbon dots, creating localized electronic states and altering the charge distribution around the defect sites [62]. These modifications enhance the composite's catalytic activity by providing more favorable sites for the adsorption and oxidation of dopamine molecules. The defects also facilitate the binding of dopamine, improving the selectivity and sensitivity of the sensor. Additionally, the heteroatoms stabilize the composite, increasing its dependability for repeated sensing applications [63]. With a wide potential window, low background currents, and quick response kinetics, the NSCQD/CoHCF composite is a promising material for advanced electrochemical sensing. The

interfacial and defect effects combine to maximize the composite's performance.

4 Conclusion

In this study, we synthesized a high-performance composite electrode using CoHCF integrated with NSCQDs derived from *Senna auriculata* biomass for dopamine sensing. Structural investigations with XRD and SEM verified the high crystallinity and production of larger hybrid clusters, showing that NSCQDs were successfully integrated, considerably improving the electrode's electrochemical characteristics. Electrochemical characterization using CV and DPV demonstrated the electrode's broad potential window, low background current, and rapid electron transfer kinetics, all critical for efficient dopamine detection. The sensor exhibited excellent linearity and high sensitivity across a dopamine concentration range of 20 to 7000 nM, achieving an ultra-low detection limit of 0.1 nM with a sensitivity of 0.01521 μA/nM. The NSCQD/CoHCF composite electrode outperformed several existing electrode materials, showcasing its promise as a reliable and effective electrochemical sensor for dopamine detection in pharmaceutical and clinical applications. The combination of high sensitivity, low detection limit, and simple fabrication process underscores its potential for real-world diagnostic use, advancing dopamine monitoring in biomedical fields.

Acknowledgements

The authors express their deep gratitude to the Central Instrumentation Laboratory at Vels University (VISTAS) for their comprehensive support throughout this research. Special thanks are extended to Sathyabama University, Chennai, for providing SEM characterization, SRM University, Kattankulathur for TEM characterization, and Pondicherry University for XPS characterization. We are particularly thankful to Dr. B. Muthuraaman, Department of Energy, University of Madras, and Dr. R. Indrajit, Department of Physics, B.S. Abdur Rahman Crescent Institute of Science and Technology, Chennai, for their invaluable guidance and persistent support in conducting this research.

Author contributions

D. Sivaguru Nathan, performed conceptualization, experimental design, methodology, formal analysis and writing—original draft. Dr. A. Padmapriya performed review and editing. M. Devendiran contributed to experimental design and data curation. Dr. R. A. Kalaivani coordinating the research activity, including planning and data validation, supervision, project administration and funding acquisition. All authors reviewed the results and approved the final version of the manuscript.

Funding

The authors have not disclosed any funding.

Data availability

All data analyzed during the study are included in this article and will be made upon reasonable request.

Declarations

Conflict of interest The author(s) declare that there is no conflict of interest regarding the publication of this article.

References

1. C. Zhang, Y. Zhou, H. Han, H. Zheng, W. Xu, Z. Wang, Dopamine-triggered hydrogels with high transparency, self-adhesion, and thermoresponse as skinlike sensors. ACS Nano **15**(1), 1785–1794 (2021)
2. G. Xu, Z.A. Jarjes, V. Desprez, P.A. Kilmartin, J. Travas-Sejdic, Sensitive, selective, disposable electrochemical dopamine sensor based on PEDOT-modified laser scribed graphene. Biosens. Bioelectron. **107**, 184–191 (2018)
3. J. Song, J. Zheng, A. Yang, H. Liu, Z. Zhao, N. Wang, F. Yan, Metal–organic framework transistors for dopamine sensing. Mater. Chem. Front. **5**(8), 3422–3427 (2021)
4. T. Qian, C. Yu, X. Zhou, P. Ma, S. Wu, L. Xu, J. Shen, Ultrasensitive dopamine sensor based on novel molecularly imprinted polypyrrole coated carbon nanotubes. Biosens. Bioelectron. **58**, 237–241 (2014)

5. S. Umapathi, J. Masud, H. Coleman, M. Nath, Electrochemical sensor based on CuSe for determination of dopamine. Microchimica Acta **187**, 1–13 (2020)
6. Q. Li, J.T. Wu, Y. Liu, X.M. Qi, H.G. Jin, C. Yang, J. Liu, G.L. Li, Q.G. He, Recent advances in black phosphorus-based electrochemical sensors: a review. Analytica Chimica Acta **1170**, 338480 (2021)
7. C.S. Liu, J. Li, H. Pang, Metal-organic framework-based materials as an emerging platform for advanced electrochemical sensing. Coordinat. Chem. Rev. **410**, 213222 (2020)
8. S.R. Prabakar, S.S. Narayanan, Catalytic oxidation of dopamine at a nickel hexacyanoferrate surface modified graphite wax composite electrode coated with nafion. Electroanal.: An Int. J. Devoted Fundam. Pract. Aspects Electroanal. **21**(13), 1481–1489 (2009)
9. S.S. Narayanan, F.A. Scholz, comparative study of the electrocatalytic activities of some metal hexacyanoferrates for the oxidation of hydrazine. Electroanal.: An Int. J. Devoted Fundam. Pract. Aspects Electroanal. **11**(7), 465–469 (1999)
10. S. Yang, G. Li, G. Wang, J. Zhao, M. Hu, L. Qu, A novel nonenzymatic H2O2 sensor based on cobalt hexacyanoferrate nanoparticles and graphene composite modified electrode. Sens. Actuators B: Chem. **208**, 593–599 (2015)
11. R. Banavath, R. Srivastava, P. Bhargava, Nanoporous cobalt hexacyanoferrate nanospheres for screen-printed H2O2 sensors. ACS Appl. Nano Mater. **4**(5), 5564–5576 (2021)
12. Q. Wang, Q. Tang, Improved sensing of dopamine and ascorbic acid using a glassy carbon electrode modified with electrochemically synthesized nickel-cobalt hexacyanoferrate microparticles deposited on graphene. Microchim. Acta **182**, 671–677 (2015)
13. S.R. Prabakar, S.S. Narayanan, Amperometric determination of paracetomol by a surface modified cobalt hexacyanoferrate graphite wax composite electrode. Talanta **72**(5), 1818–1827 (2007)
14. R. Banavath, R. Srivastava, P. Bhargava, Improved non-enzymatic H2O2 sensors using highly electroactive cobalt hexacyanoferrate nanostructures prepared through EDTA chelation route. Mater. Chem. Phys. **267**, 124593 (2021)
15. C. Chen, D. Xiong, M. Gu, C. Lu, F.Y. Yi, X. Ma, MOF-derived bimetallic CoFe-PBA composites as highly selective and sensitive electrochemical sensors for hydrogen peroxide and nonenzymatic glucose in human serum. ACS Appl. Mater. Interfaces **12**, 35365–35374 (2020)
16. P. Sun, M. Shang, R. Xie, Y. Gao, M. Tian, Q. Dai, F. Zhang, F. Chai, Dual-mode fluorimetric and colorimetric sensors based on iron and nitrogen co-doped carbon dots for the detection of dopamine. Food Chem. **445**, 138794 (2024)
17. E. Senthilkumar, A.M. Shanmugharaj, R. Suresh Babu, G. Sivagaami Sundari, K. Thileep Kumar, S. Raghu, R. Kalaivani, Development of constructed nanoporous graphene-modified electrode for electrical detection of folic acid. J. Mater. Sci.: Mater. Electron. **30**(14), 13488–13496 (2019)
18. K.T. Kumar, M.J.K. Reddy, G.S. Sundari, S. Raghu, R.A. Kalaivani, S.H. Ryu, A.M. Shanmugharaj, Synthesis of graphene-siloxene nanosheet based layered composite materials by tuning its interface chemistry: an efficient anode with overwhelming electrochemical performances for lithium-ion batteries. J. Power Sources **450**, 227618 (2020)
19. S. Shiri, N. Pajouheshpoor, H. Khoshsafar, S. Amidi, H. Bagheri, An electrochemical sensor for the simultaneous determination of rifampicin and isoniazid using a C-dots@ CuFe2O4 nanocomposite modified carbon paste electrode. New J. Chem. **41**(24), 15564–15573 (2017)
20. C.B.A. Hassine, H. Kahri, H. Barhoumi, enhancing dopamine detection using glassy carbon electrode modified with graphene oxide, nickel and gold nanoparticles. J. Electrochem. Soc. **167**(2), 027516 (2020)
21. B.K. John, T. Abraham, B. Mathew, A review on characterization techniques for carbon quantum dots and their applications in agrochemical residue detection. J. Fluoresc. **32**(2), 449–471 (2022)
22. Y. Wu, C. Li, H.C. van der Mei, H.J. Busscher, Y. Ren, Carbon quantum dots derived from different carbon sources for antibacterial applications. Antibiotics **10**(6), 623 (2021)
23. A. Padmapriya, P. Thiyagarajan, M. Devendiran, R.A. Kalaivani, A.M. Shanmugharaj, Electrochemical sensor based on N, P–doped carbon quantum dots derived from the banana flower bract (Musa acuminata) biomass extract for selective and picomolar detection of dopamine. J. Electroanal. Chem. **943**, 117609 (2023)
24. P. Arumugam, S.R. Elumali, K. Raman, A.M. Shanmugharaj, T. Purushotham, R. SubashChandrabose, Green synthesis of corn cob derived carbon quantum dots and its applications as electrolyte additive for lithium-metal batteries. ECS Trans. **107**(1), 16547 (2022)
25. S. Jing, Y. Zhao, R.C. Sun, L. Zhong, X. Peng, Facile and high-yield synthesis of carbon quantum dots from biomass-derived carbons at mild condition. ACS Sustain. Chem. Eng. **7**(8), 7833–7843 (2019)
26. Y. Hamanaka, W. Oyaizu, M. Kawase, T. Kuzuya, Synthesis of highly non-stoichiometric Cu2ZnSnS4 nanoparticles with tunable bandgaps. J. Nanopart. Res. **19**, 1–11 (2017)
27. J. Choi, J. Lee, J. Lim, S. Park, Y. Piao, PEDOT/Cobalt hexacyanoferrate free-standing films for high-performance quasi-solid-state asymmetric supercapacitor. J. Alloys Compd. **914**, 165365 (2022)

28. Y. Xiong, Y. Lin, Q. Xue, Open-framework structure-based cathode materials coupled with metallic anodes for rechargeable multivalent ion batteries. J. Electrochem. Soc. **167**, 160530 (2020)
29. V. Arunprasad, P. Siva Karthik, S. Thulasi, G.P. Arul, M. Shkir, A.T. Rajamanickam, T. Sumathi, S.R. Fredrick, Hydrothermal preparation of Ni 3 S 4/CoS 2 composite electrocatalytic materials for high performance counter electrodes of dye-sensitized solar cells. J. Cluster Sci. (2022). https://doi.org/10.1007/s10876-021-02183-5
30. X. Jiang, S. Li, G. Xiang, Q. Li, L. Fan, L. He, K. Gu, Determination of the acid values of edible oils via FTIR spectroscopy based on the OH stretching band. Food Chem. **212**, 585–589 (2016)
31. N. Jamaludin, T.L. Tan, A.S.K. Zaman, A.R. Sadrolhosseini, S.A. Rashid, Acid-free hydrothermal-extraction and molecular structure of carbon quantum dots derived from empty fruit bunch biochar. Materials **13**(15), 3356 (2020)
32. Y. Wang, R.A. Poirier, Factors that influence the CN stretching frequency in imines. J. Phys. Chem. A **101**(5), 907–912 (1997)
33. S.J. Sophia, S. Devi, K. Pandian, Cobalt hexacyanoferrate-decorated titania nanotube: CoHCF@ TNT modified GCE as an electron transfer mediator for the determination of hydrazine in water samples. Int. Scholarly Res. Notices **2012**(1), 192698 (2012)
34. V. Ivanov, D, Electrochemical properties of (Co, Fe) CN, cobaltous Prussian blue analogue. J. Solid-State Electrochem. **27**(9), 2419–2432 (2023)
35. Z.T. Pan, Z.H. He, J.F. Hou, L. Kong, B, Designing CoHCF@ FeHCF core shell structures to enhance the rate performance and cycling stability of sodium-ion batteries. Small **19**, 2302788 (2023)
36. J. Quan, E. Xu, H. Zhu, Y. Chang, Y. Zhu, P. Li, Z. Sun, D. Yu, Y. Jiang, A Ni-doping-induced phase transition and electron evolution in cobalt hexacyanoferrate as a stable cathode for sodium-ion batteries. Phys. Chem. Chem. Phys. **23**(3), 2491–2499 (2021)
37. K.K. Saravanan, P. SivaKarthik, Ru-dye grafted CuS and reduced graphene oxide (CuS/rGO) composite: an efficient and photo tunable electrode for dye sensitized solar cells. J. Cluster Sci. **31**(2), 401–407 (2020)
38. P.R. Bommireddy, M.C. Sekhar, Y.W. Lee, M. Kumar, Y. Suh, S.H. Park, Binder-free Co–Ni hexacyanoferrate as a battery-type electrode material for hybrid supercapacitors. Ceram. Int. **48**, 11849–11857 (2022)
39. Y. Zhou, C. Zhang, S. Bai, J. Su, X. Zhou, L. Zhao, Photoelectrochemical quenching-recovery biosensor based on NSCQDs/Fe2O3@ Bi2S3 for the detection of trypsin. Analytica Chimica Acta **1297**, 342361 (2024)
40. A.M. Jaramillo, R. Barrera-Gutierrez, M.T. Cortes, Synthesis, follow-up, and characterization of polydopamine-like coatings departing from micromolar dopamine-o-quinone precursor concentrations. ACS Omega **5**, 15016–15027 (2020)
41. H. Kim, G. Kim, Adsorption properties of dopamine derivatives using carbon nanotubes: a first-principles study. Appl. Surface Sci. **501**, 144249 (2020)
42. P. Manivel, M. Dhakshnamoorthy, A. Balamurugan, N. Ponpandian, D. Mangalaraj, C.J.R.A. Viswanathan, Conducting polyaniline-graphene oxide fibrous nanocomposites: preparation, characterization and simultaneous electrochemical detection of ascorbic acid, dopamine and uric acid. RSC Adv. **3**, 14428–14437 (2013)
43. T.J. Li, M.H. Yeh, W.H. Chiang, Y.S. Li, G.L. Chen, Y.A. Leu, T.C. Tien, S.C. Lo, L.Y. Lin, J.J. Lin, K.C. Ho, Boron-doped carbon nanotubes with uniform boron doping and tunable dopant functionalities as an efficient electrocatalyst for dopamine oxidation reaction. Sens. Actuators B: Chem. **248**, 288–297 (2017)
44. R.F. Brocenschi, T.A. Silva, B.C. Lourencao, O. Fatibello-Filho, R.C. Rocha-Filho, Use of a boron-doped diamond electrode to assess the electrochemical response of the naphthol isomers and to attain their truly simultaneous electroanalytical determination. Electrochim. Acta **243**, 374–381 (2017)
45. M. Amiri, E. Amali, A. Nematollahzadeh, H. Salehniya, Poly-dopamine films: voltammetric sensor for pH monitoring. Sens. Actuators B: Chem. **228**, 53–58 (2016)
46. J. Burgués, J.M. Jiménez-Soto, S. Marco, Estimation of the limit of detection in semiconductor gas sensors through linearized calibration models. Analytica Chimica Acta **1013**, 13–25 (2018)
47. A.L. Pomerantsev, D.N. Vtyurina, O.Y. Rodionova, Limit of detection in qualitative analysis: classification analytical signal approach. Microchem. J. **195**, 109490 (2023)
48. M. Lakshmanakumar, N. Nesakumar, A.J. Kulandaisamy, J.B.B. Rayappan, Principles and recent developments in optical and electrochemical sensing of dopamine: a comprehensive review. Measurement **183**, 109873 (2021)
49. L. Wu, L. Feng, J. Ren, X. Qu, Electrochemical detection of dopamine using porphyrin-functionalized graphene. Biosens. Bioelectron. **34**(1), 57–62 (2012)
50. X. Wei, Z. Zhang, Z. Wang, A simple dopamine detection method based on fluorescence analysis and dopamine polymerization. Microchem. J. **145**, 55–58 (2019)
51. Y.R. Kim, S. Bong, Y.J. Kang, Y. Yang, R.K. Mahajan, J.S. Kim, H. Kim, Electrochemical detection of dopamine in the presence of ascorbic acid using graphene modified electrodes. Biosens. Bioelectron. **25**(10), 2366–2369 (2010)

52. A. Suzuki, T.A. Ivandini, K. Yoshimi, A. Fujishima, G. Oyama, T. Nakazato, N. Hattori, S. Kitazawa, Y. Einaga, Fabrication, characterization, and application of boron-doped diamond microelectrodes for in vivo dopamine detection. Anal. Chem. **79**, 8608–8615 (2007)
53. M.H. Mashhadizadeh, T. Yousefi, A.N. Golikand, A nickel hexacyanoferrate and poly (1-naphthol) hybrid film modified electrode used in the selective electroanalysis of dopamine. Electrochim. Acta **59**, 321–328 (2012)
54. R.K. Shervedani, H.A. Alinajafi-Najafabadi, Electrochemical determination of dopamine on a glassy carbon electrode modified by using nanostructure ruthenium oxide hexacyanoferrate/ruthenium hexacyanoferrate thin film. Int. J. Electrochem. **2011**(1), 603135 (2011)
55. D.R. de Oliveira, D.S. Fernandes, D.R. do Carmo, A cerium hexacyanoferrate (III) nanoparticle-modified carbon paste electrode: voltammetric characterization and behavior in the presence of dopamine. Electroanalysis **32**(7), 1524–1532 (2020)
56. M. Yadav, P. Singh, V. Ganesan, R. Gupta, P.K. Sonkar, D.K. Yadav, In situ electrochemical synthesis of a composite film containing nickel hexacyanoferrate and bentonite clay for the sensitive determination of acetaminophen and dopamine. Electroanalysis **32**(2), 248–257 (2020)
57. M. Sajid, M.K. Nazal, M. Mansha, A. Alsharaa, S.M.S. Jillani, C. Basheer, chemically modified electrodes for electrochemical detection of dopamine in the presence of uric acid and ascorbic acid: a review. TrAC Trends Anal. Chem. **76**, 15–29 (2016)
58. H. Begum, M.S. Ahmed, S. Jeon, New approach for porous chitosan–graphene matrix preparation through enhanced amidation for synergic detection of dopamine and uric acid. ACS Omega **2**(6), 3043–3054 (2017)
59. S.S. Jeon, P.W. Kang, M. Klingenhof, H. Lee, F. Dionigi, P. Strasser, Active surface area and intrinsic catalytic oxygen evolution reactivity of NiFe LDH at reactive electrode potentials using capacitances. ACS Catal. **13**, 1186–1196 (2023)
60. A. Karmakar, S. Kundu, A concise perspective on the effect of interpreting the double layer capacitance data over the intrinsic evaluation parameters in oxygen evolution reaction. Mater. Today Energy **33**, 101259 (2023)
61. S. Raman, M. Sindhuja, Advances in silicon nanowire applications in energy generation, storage, sensing, and electronics: a review. Nanotechnology **34**(18), 182001 (2023)
62. X. Zhao, J. Wei, T. Song, Z. Wang, D. Yang, X. Zhang, F. Huo, Y. Zhang, H.M. Xiong, Computational insights into carbon dots: evolution of structural models and structure–activity relationships. Chem. Eng. J. **481**, 148779 (2024)
63. S. Lv, H. Wang, Y. Zhou, D. Tang, S. Bi, Recent advances in heterogeneous single-atom nanomaterials: from engineered metal-support interaction to applications in sensors. Coord. Chem. Rev. **478**, 214976 (2023)